2019

Development of a Fused Deposition 3D Printed Buoy and Method for Quantifying Wave Tank Reflections

Samantha G. Swartzmiller
Michigan Technological University, sgswartz@mtu.edu

DEVELOPMENT OF A FUSED DEPOSITION 3D PRINTED BUOY AND METHOD FOR QUANTIFYING WAVE TANK REFLECTIONS

By

Samantha G. Swartzmiller

A THESIS

Submitted in partial fulfillment of the requirements for the degree of

MASTER OF SCIENCE

In Mechanical Engineering

MICHIGAN TECHNOLOGICAL UNIVERSITY

2019

This thesis has been approved in partial fulfillment of the requirements for the Degree of MASTER OF SCIENCE in Mechanical Engineering.

Department of Mechanical Engineering – Engineering Mechanics

Thesis Advisor:	*Dr. Gordon G. Parker*
Committee Member:	*Jay Meldrum*
Committee Member:	*Dr. Wayne W. Weaver*
Department Chair:	*Dr. William W. Predebon*

Table of Contents

List of figures

List of tables

Acknowledgements

Thank you Jay Meldrum, for convincing me to go for a master's degree.

Thank you Dr. Gordon Parker, for taking me on as a graduate student and your guidance.

Thank you Bob Page and the 6th floor shop guys, for sharing your expertise.

Thank you Dr. David Forehand, for help in brainstorming concepts for this work.

Thank you Dr. Enrico Anderlini, for assistance in properly operating the wave gauges.

Thank you Dr. Umesh Korde, for providing the foundation of my wave energy education.

Thank you God, for all the ways you have blessed me along the way.

Abstract

Testing model scale prototypes is integral to the development of wave energy converter (WEC) technology. Model scale WECs are tested in wave tanks where they are subjected to repeatable wave fields. Their presence in water creates radiated waves that eventually reflect off tank walls disrupting the intended wave field. Fabrication of model scale WECs is another developing aspect of tank testing. Often model WECs are built of foam. Additive manufacturing is a promising alternative although the most common method, fused deposition modeling (FDM) 3D printing, does not typically produce waterproof parts. The goals of this work were 1) develop a method to characterize tank reflections on a model specific basis and 2) develop an efficient and economic method for creating FDM 3D printed model WECs. A spherical physical model buoy was developed to act as both an actuator and sensor to quantify reflections in a circular tank. In conjunction with a calibrated computational model, it detected and quantified changes in reflections caused by varying damping treatments applied to tank walls. A waterproofing technique for FDM 3D printed buoys was found. This work demonstrates that damping treatments can be tuned on a model specific basis prior to tank testing through the use of WEC model surrogate buoys, and that these surrogate buoys can be efficiently and economically produced using the widely available technology of FDM 3D printing.

1 Introduction

The following sections cover relevant literature related to hydrodynamic modeling, physical modeling, and physical testing of model scale WECs. Additionally, the objective of this work is introduced.

1.1 Literature Review

The most common approach to numeric hydrodynamic modeling WECs is using linear potential theory [1]. Assumptions made in linear potential theory are 1) the waves have small amplitudes relative to their length, 2) there are small deflections, 3) small forces, 4) incompressible flow [1], [2]. Linear hydrodynamic models are a simplification but allow for the important convenience of Fourier analysis used in all hydrodynamic boundary element method (BEM) modeling software [1].

There are multiple hydrodynamic boundary element model (BEM) software available such as WAMIT, NEMOH, and AQWA. WAMIT was used for frequency domain analysis in this research. WAMIT was developed by MIT in the 1980's [3]. It is "based on linear and second-order potential theory for analyzing floating or submerged bodies, in the presence of ocean waves" [3]. The outputs of WAMIT can be transformed from frequency to time domain to be used in time domain models. Time domain models can then be experimentally verified.

Model scale WEC are commonly used in wave tanks in order to carry out experimental testing. Model scale WECs are typically crafted from a combination of foam and off the shelf PVC and metal components [4], [5], [6], [7], [8], [9], [10]. Fiberglass and rubber have been used as well, but not as often [11], [12]. Laminating foam boards together to create larger and stronger shapes is a method used by University of Edinburgh, a prominent WEC research group [9].

Additive manufacturing is often used to fabricate turbines used in oscillating water column model WECs [4], [13], [14], [15]. 3D printing is sometimes used to create a part or two in a typical model WEC composed of mostly foam, PVC, and metal [16], [17], [18], [19]. Rarely is it used to print an entire model WEC. Only one study was found using a model WEC that was composed of a fully 3D printed unit [20]. It was constructed from two 3D printed hemispheres of diameter 0.136 m. Inset screws held the halves together. A double o-ring seal was used to waterproof the seam, and with that the 3D printed sphere was wave tank ready.

Due to space restrictions, wave tanks in which model WECs are tested are finite in nature. Tank walls reflect waves. Reflections can have a positive or negative consequence on the built wave field but conventional WECs are designed for offshore locations, meaning no reflection features for miles [21]. Reflections can be a significant problem in wave tank experiments [22]. "For reliable experimental data, the reflection from the rigid end wall should be less than 5–10% of the incident waves" [22]. Additionally, high levels

of wave reflection can cause long wait times between experiments while the tank becomes still [23]. Quantifying and subsequently reducing the amount of reflections in a wave tank is critical for longer experiments and reliable data [22]. Therefore it is advantageous for wave tanks to mimic non-reflective environments.

Some tanks are designed long and narrow. The waves are made at one end of the tank and travel to the other. The model WEC is placed near the wave makers and the experiment is limited to run until the reflected waves make their way back to the floating body. There are other wave tank geometries, like the Edinburgh curved tank, but there is still a need for wave damping to reduce tank reflections. This can be done actively or passively. Actively, the same paddles that produce the waves also absorb them with a prescribed damping motion [24]. Passively, there are multiple methods. A beach like structure, like a submerged wedge, can be placed at the end of the tank at which the waves are directed [19], [20], [25]. The beach causes the waves to break. Damping material can be applied to the walls of the tank such as sponge material or perforated plates [22], [23], [25], [26]. A combination of the two can be used in the form of a perforated beach [21]. The curved wave tank at the University of Edinburgh utilizes an active-passive combination of a 90 degree arch of "absorbing-wavemaker paddles" and a wall lined with wedge shaped foam and woven PVC blocks as an efficient damping scheme [23]. Whatever the wave tank shape, imitating infinite bounds by damping reflected waves is desired [25].

1.2 Objective

The objective of this work were 1) develop a method to characterize tank reflections on a model specific basis and 2) develop an efficient and economic method for creating FDM 3D printed model WECs.

2 Modeling

A second order time domain model was developed using MATLAB and Simulink to simulate the vertical (e.g. heave) motion of an oscillating body in water. The vertical motion of a body oscillating in water can be likened to a mass spring damper system. The simulation was based on the following equation of motion which is also used as the equation of motion of a mass spring damper.

$$m\ddot{x} + c\dot{x} + kx = F_e(t)$$

Buoy movement was initiated by release from an initial displacement of 0.01m, not an external excitation force, therefore excitation force was set to zero. The equation of motion was then rearranged to solve for vertical acceleration ($\ddot{x}$) and integrated twice to find vertical displacement (x). A state space representation of this is shown below

$$x_2 = \dot{x}$$

$$\dot{x_1} = x_2$$

$$\dot{x_2} = -\frac{c}{m}x_2 - \frac{k}{m}x_1 + \frac{F_e}{m}$$

$$x = Ax + bF_e(t) = \begin{bmatrix} 0 & 1 \\ \frac{-k}{m} & \frac{-c}{m} \end{bmatrix} x + \begin{bmatrix} 0 \\ \frac{1}{m} \end{bmatrix} F_e$$

The damping constant (c) and hydrostatic stiffness (k) are both hydrodynamic coefficients. Damping has two sources, radiation and viscous where viscous damping is often neglected [27]. Therefore c is equal to purely radiation damping. Total mass (m) is made up of two parts, mass of the buoy (M), and added mass (m_a) due to the fluid that moves with the body.

$$m = M + m_a$$

The simulated and experimental displacements were compared by calculating the integral square error between them. The integral square error was used quantify the deviation of the simulated displacement from the experimental.

The simulation differed from the experiment in that it did not model reflections from the tank walls and their effect on buoy motion. The simulation was designed to model the buoy's initial displacement and the vertical oscillations immediately following its release. It does not model the buoy's motion once waves are reflected off tank walls back towards the buoy, thus affecting the buoy's motion. Due to the small size of the thank, this means there is only a short time window in which the simulation is designed to accurately predict the buoy's motion.

2.1 Hydrodynamic Parameters

2.1.1 WAMIT

WAMIT is a hydrodynamic modeling tool developed by MIT [3]. WAMIT uses boundary element method under linear potential flow theory to estimate hydrodynamic coefficients used for numerical modeling of WECs [1]. For this application, WAMIT was used to estimate added mass and radiation damping terms in frequency domain, as well as hydrostatic stiffness. The input parameters for this analysis in WAMIT were: buoy geometry, mass, water density, and depth. A water density of 1000 $\frac{kg}{m^3}$ was used. All hydrodynamic parameters found with WAMIT were calculated for the infinite domain case. Infinite domain indicates the buoy was in an unbounded fluid, no reflecting walls (i.e. waves radiate to infinity) and deep water.

2.1.2 Added Mass

Added mass is representative of the water directly surrounding a buoy's submerged surface [27]. This water is accelerated when the body oscillates, adding mass to the buoy. For a body at the free surface, that is floating, partially submerged in water, added mass has both a frequency dependent and non-frequency dependent term [27].

2.1.3 Radiation Damping Coefficient

The radiation damping coefficient is representative of the viscous losses from the buoy to the surrounding water at the boundary layer [27]. The radiation damping coefficient can be found using WAMIT but in this work an equivalent transfer function, shown below, was used to calculate the infinite domain value for radiation damping. F_r is radiation force and $\dot{x}$ is vertical velocity of the buoy.

$$\frac{F_r}{\dot{x}} = \frac{1}{m} \cdot \frac{248.3s^3 + 975.7s^2 + 4355s + 7390}{s^4 + 15.45s^3 + 117.6s^2 + 363.5s + 1244}$$

2.1.4 Hydrostatic Stiffness

Hydrostatic stiffness is the spring constant of the buoy's equation of motion. It is caused by the buoyancy of the buoy and is assumed constant for small deflections [27]. Hydrostatic stiffness was found using WAMIT.

2.1.5 Comparison of WAMIT Results to Havelock

Added mass and radiation damping were solved for analytically using Havelock's method published in 1955 [2]. Havelock's method was also completed under an infinite domain assumption. Figure 1 below shows a comparison of WAMIT and Havelock's

calculations for non-dimensional added mass (j) and radiation damping coefficient (h) for a floating, oscillating sphere in infinite domain. It should be noted that the radiation damping coefficient plotted in figure 1 is doubled ($2h$) for easier visual comparison. A vertical line at the experimental non-dimensional frequency of 1.08 is shown in green in figure 1.

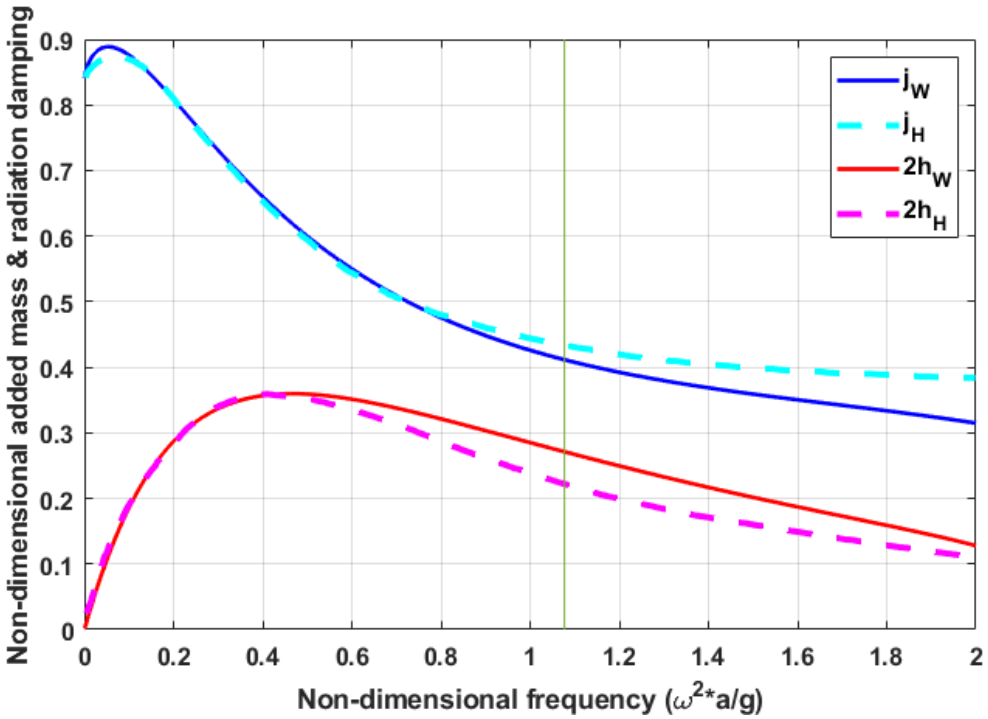

Figure 1. Comparison WAMIT and Havelock computed frequency dependent non-dimensional added mass (j) and radiation damping ($2h$) of a floating, oscillating sphere in infinite domain

The following equations describe how non-dimensional added mass and radiation damping are related to physical values. Density of water is denoted by ρ and radius of the body by a.

$$m_a = \frac{2}{3}\pi\rho a^3 j$$

$$c = \frac{2}{3}\pi\rho a^3 \omega(2h)$$

The hydrodynamic parameters added mass and radiation damping were confirmed by Havelock's work in a general sense but as much as 20% error seen at the frequency of interest pointed to the need for hydrodynamic parameter calibration for the specific model being used. The WAMIT values were used as a starting point for tuning the simulation.

2.2 Tuning the Simulation

Experimental motion data of the buoy was plotted against simulated buoy motion. In comparison, the simulated data was clearly overdamped and out of phase. This can be seen in figure 2.

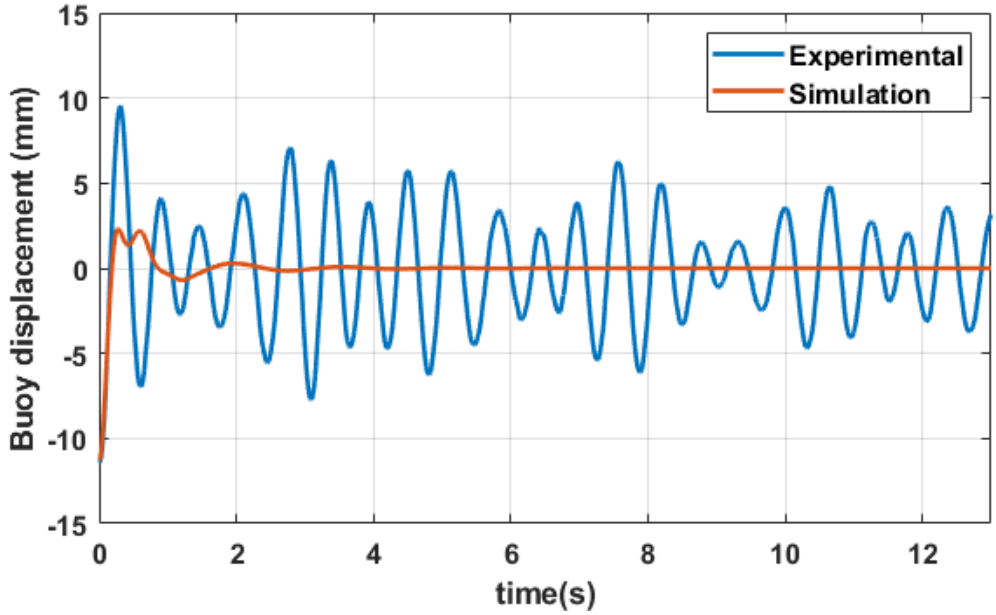

Figure 2. Example of experimental data and WAMIT tuned simulation

The hydrodynamic parameters from WAMIT, found for infinite domain, did not characterize the system well. This was expected because the experimental data was collected in a tank of finite domain (depth 0.4 m, diameter 0.19 m); the infinite domain WAMIT solution served as a starting point. The simulation was tuned to match the experimental data by finding new, optimal hydrodynamic parameters. Radiation damping and added mass were divided my total mass to form two optimization parameters, $\hat{c}$ and $\hat{k}$, shown below.

$$\hat{c} = c/(M + m_a)$$

$$\hat{k} = k/(M + m_a)$$

These parameters were optimized for one second, equal to 1.67 periods. Optimizing the hydrodynamic parameters captured all the physics with the only assumption being that the buoy had a second order linear response. The simulation did not model the reflected waves' effect on the buoy, therefore the optimization was stopped at the time where reflected waves began to affect the buoy's motion (t_b). The time between buoy release (t_1) and t_b was estimated as one second based on the average time of phase shift

between simulated and experimental data. The original and optimized values for $\hat{c}$ and $\hat{k}$ are shown below in table 1.

Del was another variable included in the optimization. Del represented the difference between the ideal initial displacement of the buoy (1 cm) and the actual displacement found in experimental data. The initial buoy displacement was not identical in all three experiments because the entire test set up had to be taken apart to apply more wall damping between experiments. Each time the experimental set up was rebuilt, it brought a slight variation of initial buoy displacement. The introduction of the variable del was important because it allowed the simulation to adjust initial displacement to match the experiment. Del was never larger than 1.3 mm. The optimized values are shown below in table 1.

Table 1. Comparison of WAMIT vs. optimized hydrodynamic variables

	WAMIT	**No damping**			**Damping 1**			**Damping 2**		
Test #	-	One	Two	Three	One	Two	Three	One	Two	Three
Del (mm)	0	-1.3	-1.2	-1.3	-0.37	-0.29	-0.23	-0.39	-0.076	-0.031
$\hat{c}$ $(\frac{1}{s})$	11.4	2.93	2.90	3.25	3.07	3.13	3.10	2.78	2.74	2.78
$\hat{k}$ $(\frac{1}{s^2})$	171.2	171.3	184.0	190.0	186.6	175.7	179.0	175.9	172.0	178.3

3 Experiments

The goal of the experimental testing was twofold. The first goal was to validate the concept of using a buoy as both an actuator and a sensor in order to quantify reflections in the tank. The second goal was to identify whether a specific damping treatment (10 pores per inch (PPI) reticulated polyurethane foam) applied to tank walls could alleviate reflections, bringing a finite domain experiment closer to infinite domain conditions. If so, this reduction in reflection would also be characterized. The buoy had two main functions. First, it acted as the wave maker. Second, it oscillated freely to act as a sensor.

3.1 Wave Creation Method

A repeatable method of wave creation was necessary for this experiment. The buoy's initial condition response was used to create waves. The buoy, a weighted sphere (9.5 cm radius) was pulled 1 cm below its natural draft of 9 cm and held there until the buoy and water surface were still. A manual quick release mechanism was used to release the buoy creating waves that emanated from the buoy at the center of the polycarbonate inner ring.

3.2 Buoy

3.2.1 Design

Geometrically, the buoy was designed as a point absorber. A point absorber is characterized by being omni-directional, axisymmetric, and typically oscillating vertically (heave)[27]. Point absorbers are specifically of interest for WEC array applications due to their small size and easy to mass produce shape [27]. The simple shape of typical point absorbers, sphere or cylinder, provided a good starting point for fabricating a 3D printed model. The final buoy was printed as a sphere.

The diameter of the buoy was limited to 19 cm due to the bed size of the 3D printer. The wall thickness was 0.64 cm. Inside the buoy there was a post around which lead weights were placed as ballast. The post was printed hollow and later tapped to allow the insertion of a screw. A screw and washer held two lead weights in place at the bottom of the buoy. The top of the buoy featured a removable, circular lid with handle. The lid opening was waterproofed using a press-fit o-ring seal.

3.2.2 Fabrication

After the buoy was printed using the most widely used form of 3D printing, FDM, some additional post processing was required. The printing tolerance of the 3D printer was larger than the amount by which the press fit lid was undersized to fit inside the opening. In order to get the lid to fit it was machined down with a lathe. The groove in which the o-ring sat had remaining structural plastic that was not dissolved and washed away during

the washing process. The remaining structural plastic inside the o-ring groove was quickly chipped away using a small pointed tool. The hollow center post inside the buoy needed to be tapped to allow the insertion of a screw. This was completed using a hand tapping tool. The buoy was then waterproofed with spar urethane spray. This process is detailed below. Last, a mooring feature was attached to the bottom of the buoy allowing it to be actuated up and down in the water. This feature was designed to be unobtrusive so as to not affect the shape or geometry of the buoy. A loop of high strength, no stretch, braided fishing line was attached to the very bottom of the sphere with a donut shaped plastic patch and epoxy. This created a location from which a line could be attached and the buoy could be evenly displaced downward below its natural draft.

Additional parts were used in the assembly of this 3D printed buoy. A commercial, off the shelf $\frac{1}{16}$ inch thick (0.16 cm), 3.5 inch inner diameter (8.9 cm) ethylene propylene diene monomer (EDPM) rubber o-ring was used to waterproof the opening of the buoy. Two 1.25 lb (0.57 kg) lead disc weights were used as ballast inside the buoy. A steel screw and washer were used to secure the lead weights in place. A loop of braided fishing line was attached to the very bottom of the sphere. Seven Qualysis motion tracking balls were fixed to the top of the buoy to allow for motion tracking. The total weight of the buoy was 1.595 kg. A cross sectional of the buoy assembly can be seen in figure 3.

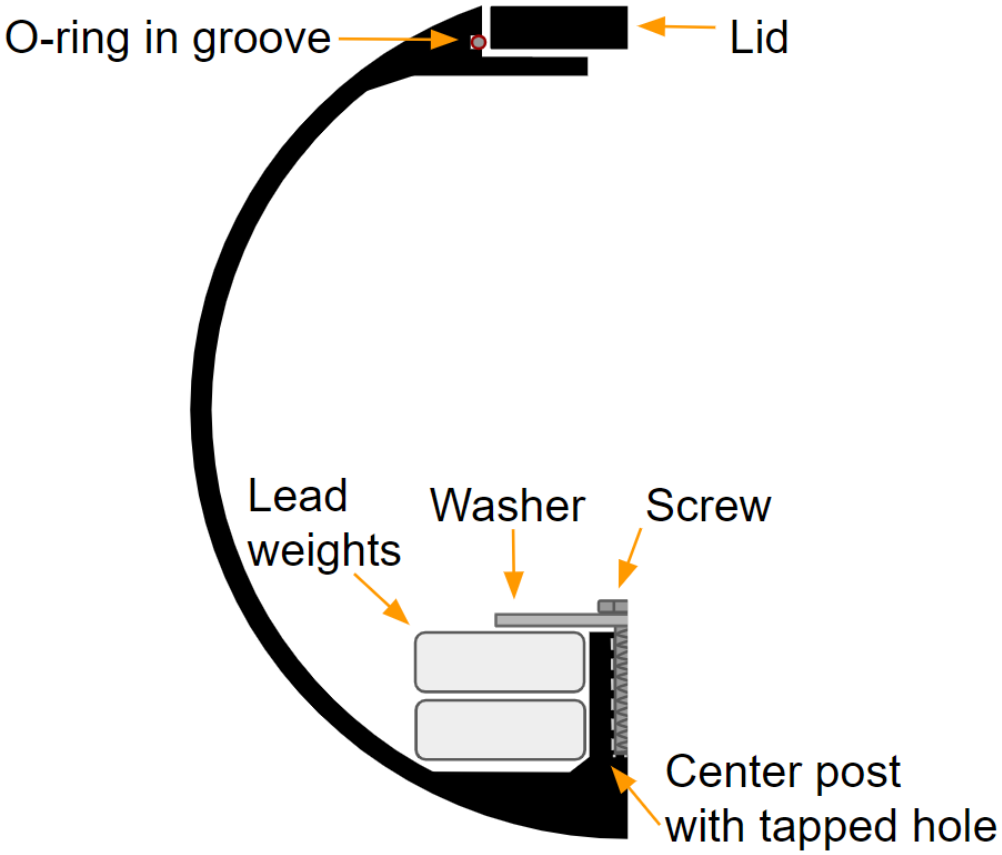

Figure 3. Cross section drawing of buoy assembly

3.2.3 Waterproofing

FDM 3D printing with ABS plastic does not produce watertight parts. For this reason it was necessary to find a product to coat the surface of the 3D printed buoy to waterproof it. This is not a common procedure so the solution was found via trial and error. There were four requirements that the waterproofing scheme needed to satisfy.

1. Even application so as to not change the smooth, spherical geometry
2. Nonreactive with ABS plastic
3. Applicable to small or intricate geometries (e.g. handle)
4. Create a watertight coating on the 3D printed parts

After testing three different products, Minwax Indoor/Outdoor Helmsman Spar Urethane Aerosol spray met all requirements. Seven coats of spray were applied to the sanded surface of the 3D printed parts and allowed to cure. The finished buoy is shown in figure 4.

Figure 4. Front and top view of buoy

3.3 Experimental Setup

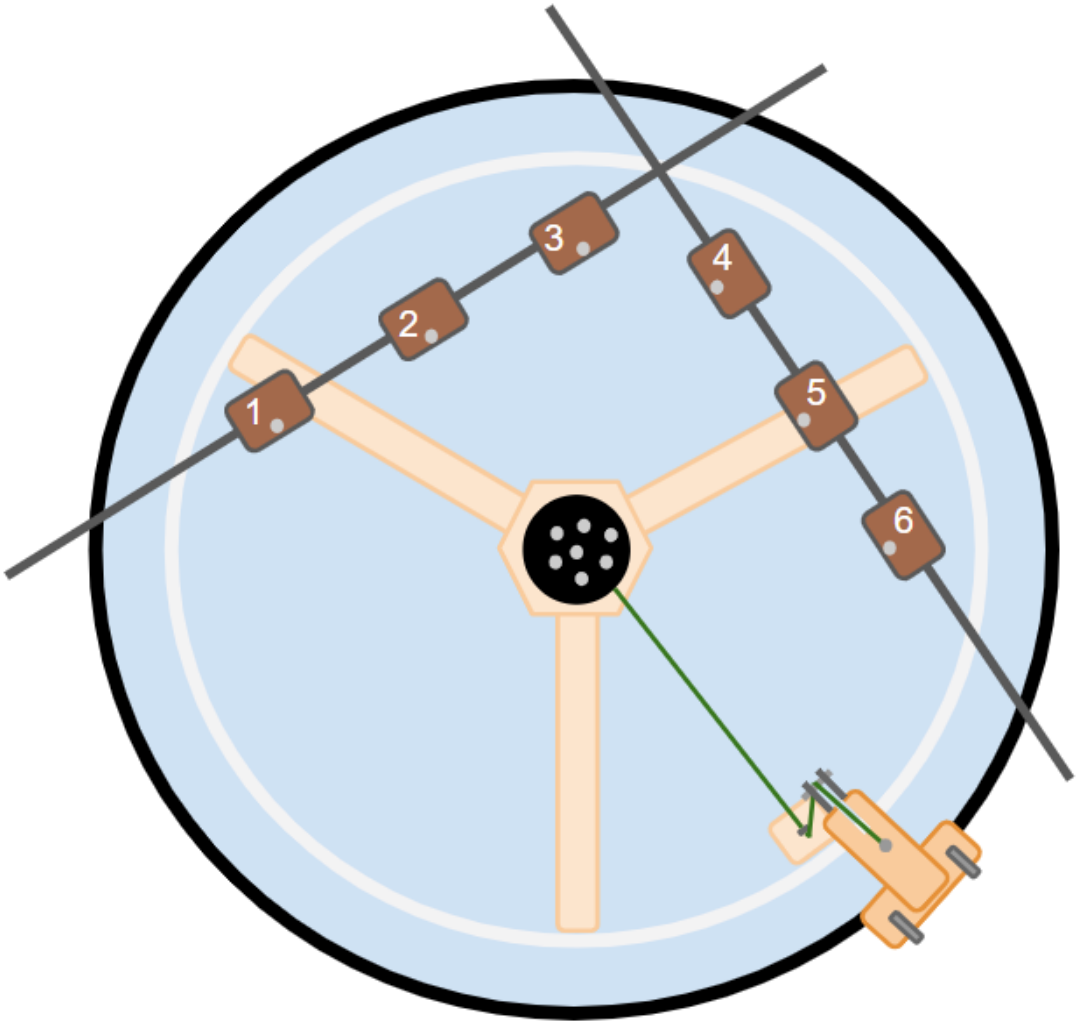

Figure 5. Diagram of experimental setup

Figure 5 above shows a top view drawing of the experimental test setup. The wave tank used for these experiments was a 300 gallon Rubbermaid agricultural water tank. The water depth was 0.4 m. Inside of the tank was a polycarbonate cylinder (0.58 m radius, 0.61 m height) creating an inner ring off which waves reflected. For these experiments it was desired that the reflecting surface be strictly vertical. The Rubbermaid tank had stepped sidewalls and therefore was not strictly vertical. A better reflecting surface was made by inserting the polycarbonate ring inside the tank.

A three prong wooden brace was weighted to the bottom of the tank. This brace identified the center of the inner ring and helped the polycarbonate inner ring stay in place.

Two bars of 80-20 aluminum rod were suspended above the tank, each fitted with three Edinburgh Design wave gauges. The wave gauges extended down into the water below without touching the bottom. They measured wave elevation with an accuracy of 1 mm. The distance between gauges 2 and 5 and the inner wall was equal at 15.6 cm. The distance between wave gauges was 30.5 cm.

The buoy was suspended in the middle of the tank. The buoy was attached to an eye bolt pulley directly below it with high strength, no stretch, braided fishing line. The line was directed outward to a second eye bolt pulley positioned next to the inner wall. The line threaded upwards to a quick release mechanism attached to the sidewall of the tank. The quick release mechanism allowed the buoy to be held below its natural draft and then released to create an impulse wave emanating from the buoy at the center of the tank.

The buoy was outfitted with seven motion tracking balls, all located near the top of the buoy. A series of 8 Qualysis motion tracking cameras, along with Qualysis software, was used to track the 6 DOF movement of the buoy. A motion tracking ball was placed on the top of each wave gauge in order to identify its relative position to the buoy.

3.4 Experiment Design

In order to understand if the buoy could be used as both an actuator and a sensor to quantify reflections in the tank, three experiments were conducted with varying levels of damping treatment on the walls of the inner polycarbonate ring.

1. "No wall damping" No damping treatment on inner walls
2. "Damping 1" First layer of 0.5 inch (1.27 cm) thick 10 PPI reticulated polyurethane foam adhered to inner walls
3. "Damping 2" Second layer of foam added, total wall damping thickness of 1 inch (2.54 cm)

Three tests were completed for each experiment, resulting in nine sets of data. Each test was 15 seconds long. Each 15 second test could be split into three sections.

1. *Still water*: buoy held still 1 cm below its natural draft
2. *Radiated waves*: buoy released from its partial submersion to oscillate freely, creating a ring of radiated waves
3. *Reflected waves*: radiated waves hit tank walls and reflect back towards the center. Reflected waves change the wave field and the buoy's motion

These three sections are represented in the timeline in figure 6. The timeline of one test seen in figure 6 is marked by seven events. Wave height data collection begins at t_{0_wg}. Within 1-3 seconds buoy motion data begins at t_{0_bm}. The buoy is released at t_1, marking the start of radiated waves. The radiated waves hit the wave gauges at t_{wg1}. Radiated

waves hit the tank walls at t_r and are transformed into reflected waves directed back towards the center of the tank. The waves pass by the wave gauges again a t_{wg2} and finally hit the buoy at t_b. As stated in section 2.2, t_b is the time where reflected waves begin to affect the buoy's motion.

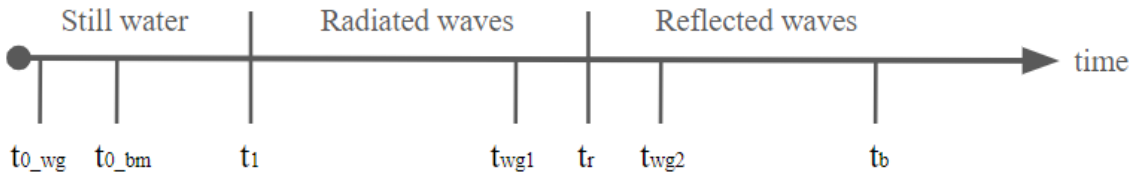

Figure 6. Timeline of events within one test

By observation it is hypothesized that radiated waves last for only 1-2 seconds, after which the experiment is expected to diverge from the simulated model which does not contain reflecting walls.

4 Results

4.1 Repeatability in Wave Creation

After testing the buoy's initial condition response in the wave tank absent of any damping treatment, the method of wave creation was proven to be repeatable. The repeatability is evident in both the buoy motion (figure 7) and wave height data (figure 8). Using test 1 as reference, the maximum error in buoy motion between the three tests was 1.3 mm. The average error was 0.2 mm. The maximum error in wave height between the three tests was 0.5 mm. The average error was 0.05 mm.

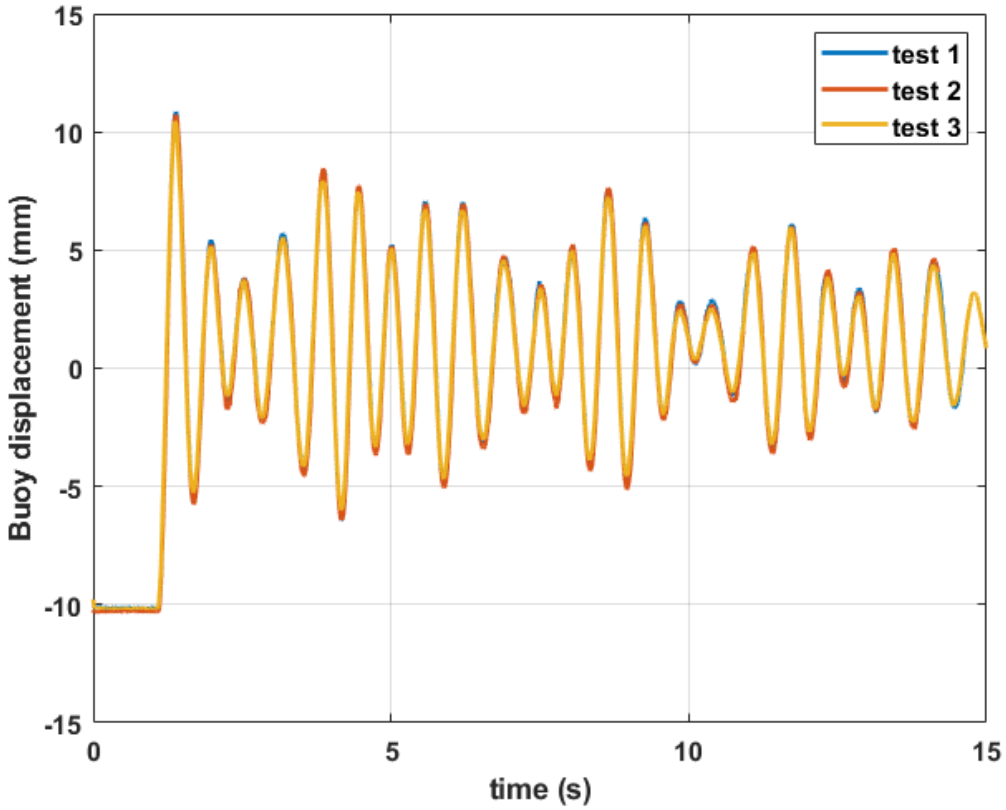

Figure 7. Buoy motion of initial condition response (3 data sets), no wall damping

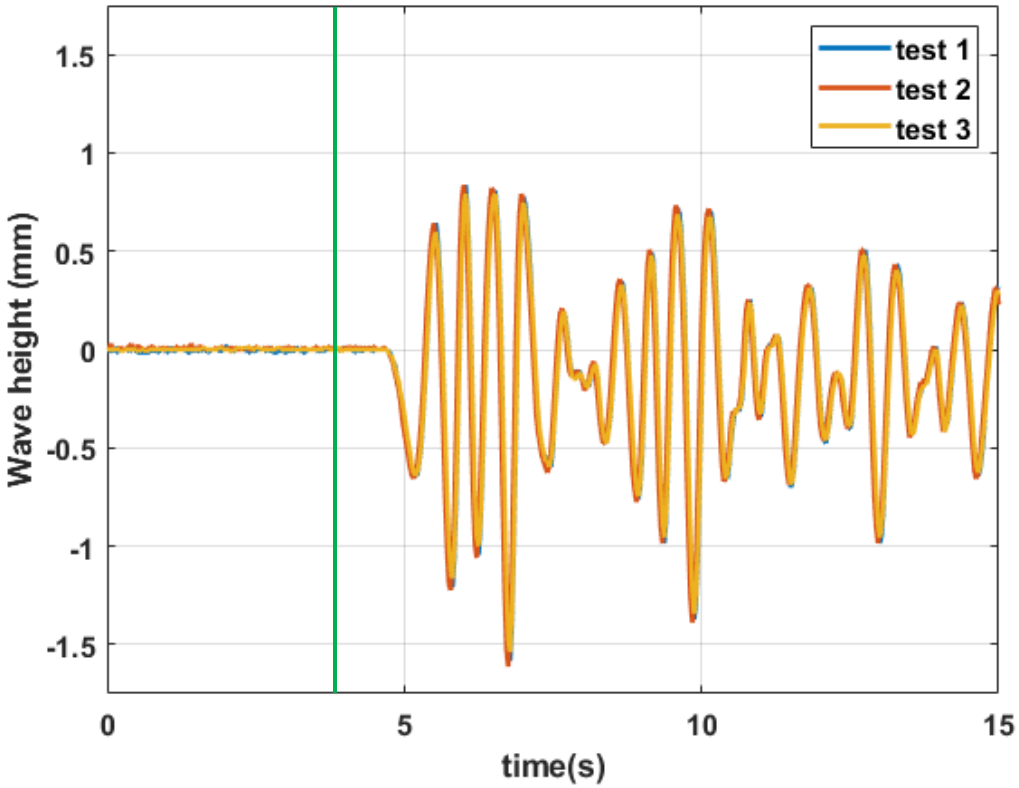

Figure 8. Wave elevation caused by initial condition response of buoy (3 data sets), no wall damping

In figure 7, t_1 (the time the buoy was released), occurs at approximately 1 second. In figure 8, t_1 is approximated by the green line at 4 seconds. May it be noted that events such as buoy release do not align on the time axis because wave data collection was started 0-3 seconds before motion data collection.

4.2 Buoy Motion

The buoy motion from the no wall damping experiment can be seen in figure 7 in the previous section, with one layer of damping treatments in figure 9, and a second layer of damping in figure 10. The three tests from each experiment lay directly on top of one another in figures 7, 9, and 10. This shows that wall damping thickness does not affect the repeatability of the experiment.

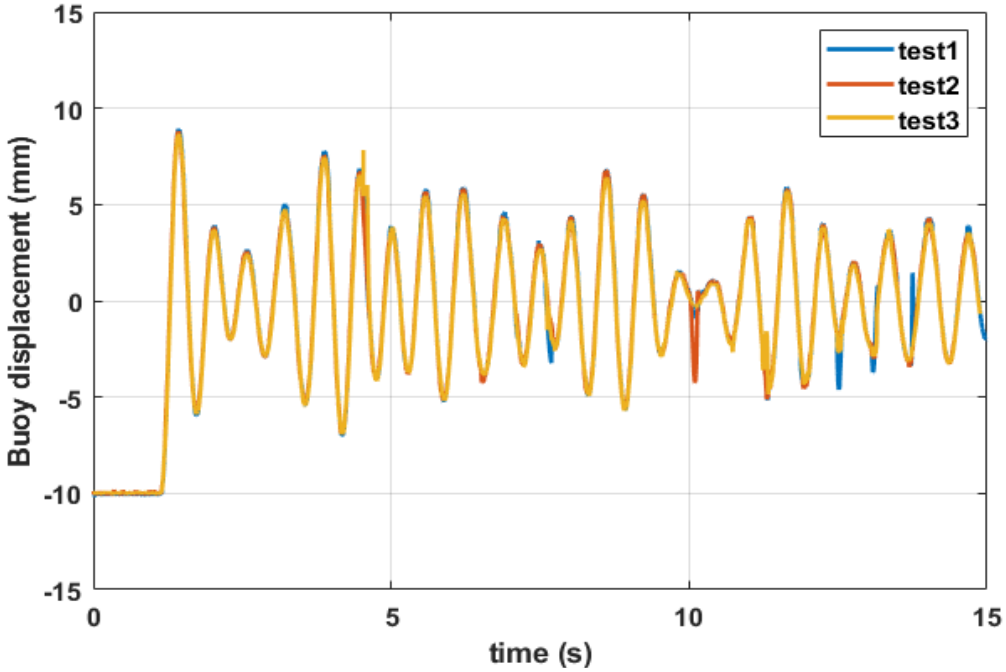

Figure 9. Buoy motion of initial condition response (3 data sets), damping 1

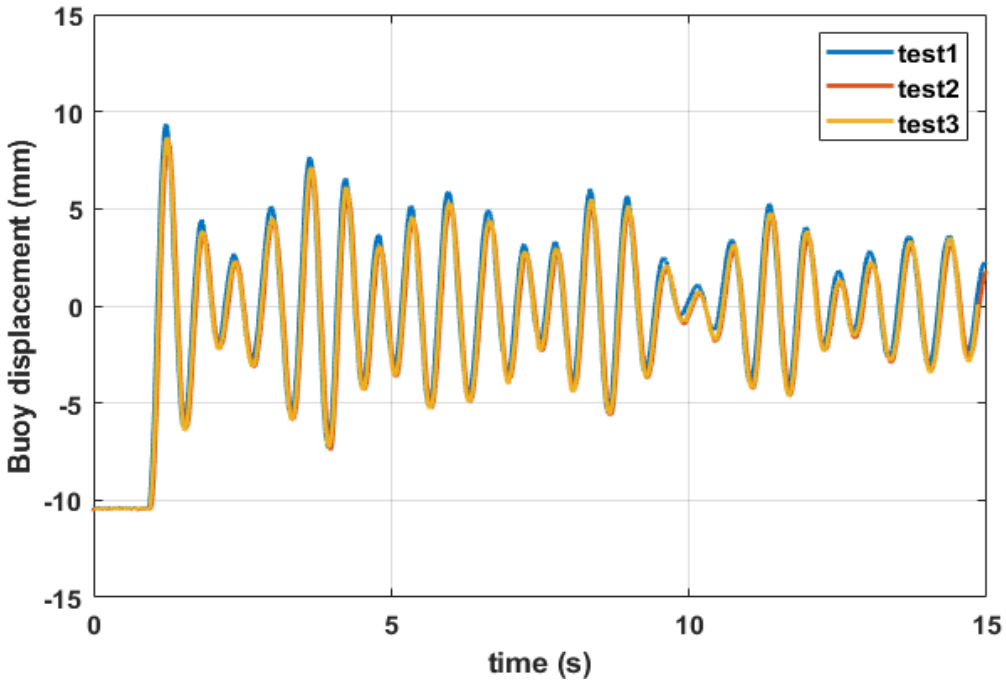

Figure 10. Buoy motion of initial condition response (3 data sets), damping 2

Test one from each experiment (no wall damping, 1 layer, 2 layers) is overlaid in figure 11. It is difficult to visually identify if increased wall damping decreased buoy motion from this plot. The change in reflections due to damping treatments is quantified in the following section 4.3.

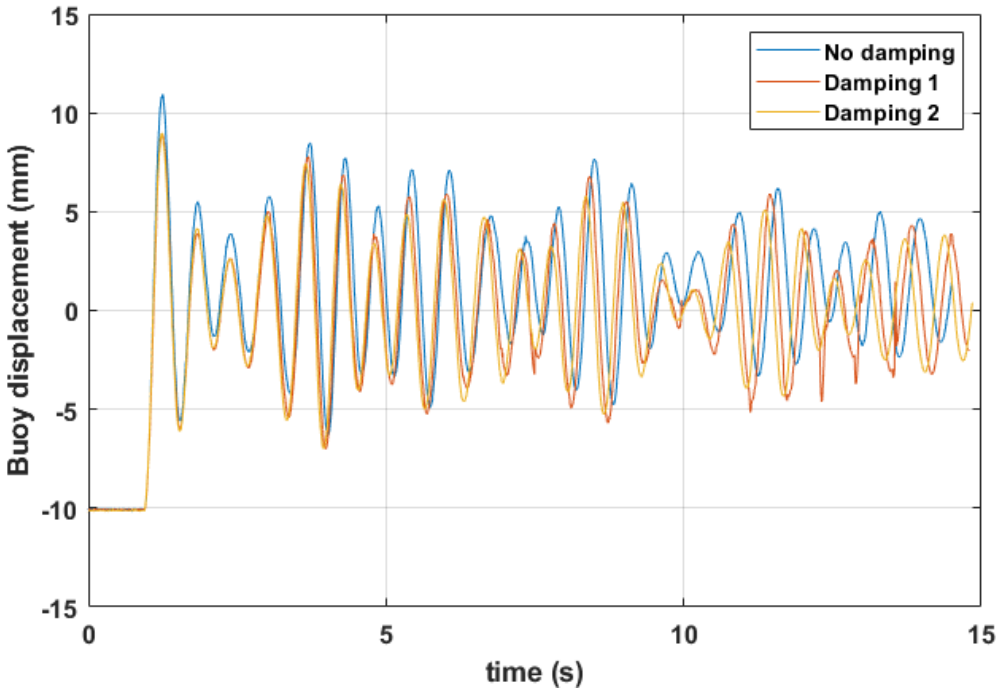

Figure 11. Buoy motion of initial condition response from test 1 of no wall damping, damping 1, and damping 2

4.3 Simulation and Quantifying Reflection

The tuned simulation produced buoy motion that closely matched the experimental data for the first 1-2 seconds. After this time, experimental reflections excited the buoy and it continued to significantly oscillate. In the simulation, the absence of reflected waves allowed damping forces to quickly bring the buoy to rest. This differences between experimental and simulated buoy behavior can be seen in figure 12.

The average integral square error (ISE) between experimental and simulated data, shown in figure 13, was used as a metric to quantify the divergence of the experimental buoy motion from the simulated. An inverse relationship between ISE and wall damping thickness was expected, that is, as wall damping increased, the difference between experimental and simulated buoy motion would decrease.

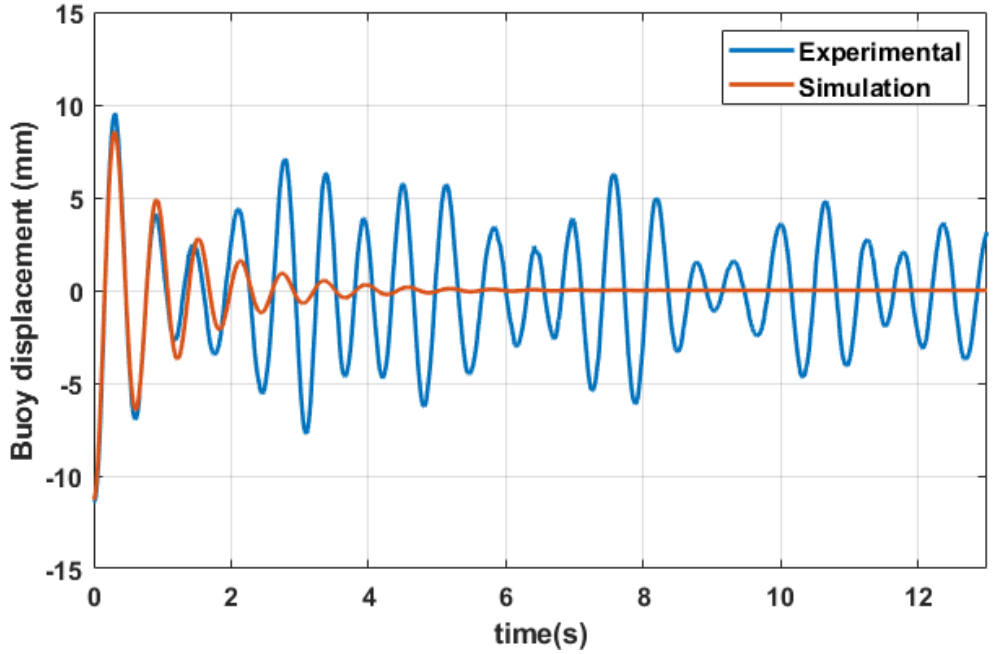

Figure 12. Simulated buoy motion compared to experimental (no wall damping, test 1)

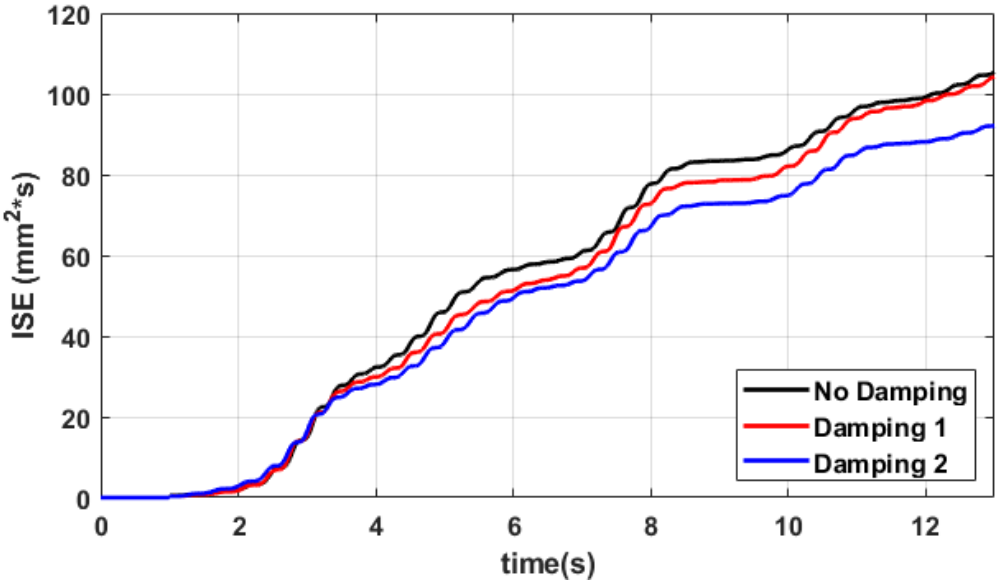

Figure 13. Average ISE between experimental and simulated buoy motion from three experiments (no wall damping, damping 1, damping 2)

Figure 14 shows the normalized average ISE from the three experiments. Normalized ISE was calculated by dividing ISE by time. The trends seen in figure 13, average ISE, are more pronounced after normalizing. The average change in normalized ISE between no

wall damping and damping 1 during the time interval 4-13 seconds is -0.16 mm^2. The average change between damping 1 and damping 2 is -0.62 mm^2.

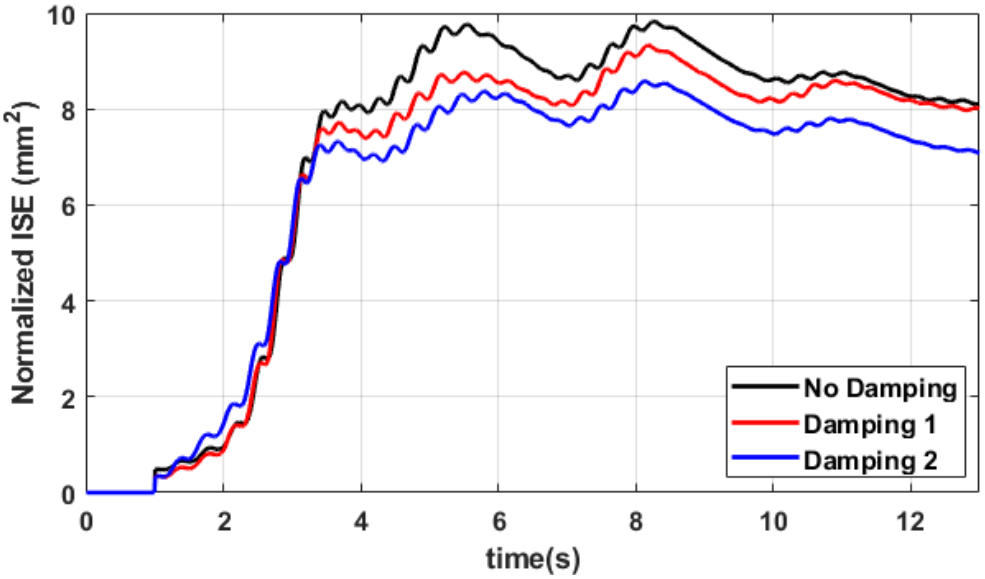

Figure 14. Normalized average ISE between experimental and simulated buoy motion from three experiments (no wall damping, damping 1, damping 2)

5 Discussion

5.1 3D Printing Improvements for Model WECs

Creating WEC prototypes to test in wave tanks is no easy task. WEC prototypes must be waterproof and highly buoyant. In the past it has been common practice to meticulously carve buoys out of foam [9]. There are a few problems that arise with foam models.

1. Harder, meticulous manufacturing process
2. Difficult remodeling process for prototype iteration
3. Exact geometric representation is not available
4. Difficult to create encapsulating shapes to protect wireless electronics
5. Rigid foam is fragile

The first and second have to do with model creation and iteration. If any changes need to be made to the buoy, creating a second foam prototype is as hard as it was the first time around. It is ideal to know the exact shape and dimensions of a prototype but the processes by which a foam model is made do not lend themselves well to that. It is common to have electronics on board that need to be protected from water. Ideally these are wireless electronics because long wires produce parasitic losses that can overpower the small scale at which WEC prototypes function. They also get in the way of the buoy's motion [9]. Encasing anything in foam is a difficult task and involves carving out caverns to fit whatever needs to go inside. Foam models aren't typically made from foam as fragile as polystyrene but even stronger rigid foams that are laminated together easily bruise with impact [9].

FDM 3D printing stands as an efficient and cost effective method for prototyping model scale WECs. It has the ability to improve all five major issues with foam modeling.

1. Automated manufacturing process
2. Clear and easy workflow established for remodeling/reprinting
3. CAD file available
4. Easy to create buoyant, encapsulating shapes
5. Plastics used in 3D printing are more robust than rigid foam

Budding WEC research groups can easily adopt this tool for model making due to its prevalence in research and technical settings. Even research groups with developed model making procedures can benefit from FDM 3D printing for tasks such as the quick production of prototype surrogates for tuning model specific damping treatments, as was shown in this work. As stated earlier, it is likely that they already have access to this technology because it is the most widely utilized form of additive manufacturing [28].

The major issue that stands in the way of FDM 3D printing model scale WECs is waterproofing. Expensive 3D printers have the precision to print watertight; not every

research group has access to these kinds of printers. There is no existing workflow or prescribed method for creating a waterproof FDM 3D printed buoy. In this work an efficient, economic, and readily available method is developed to waterproof FDM 3D printed buoys.

5.2 Reflections

The predicted relationship between wall damping thickness and ISE was observed and can be seen in figure 13 of section 4.3. The metric, ISE, which quantifies reflection, drops when foam is added to tank walls. This is why the black (no wall damping) line is higher than the red (damping 1) and the red is higher than the blue (damping 2) line, but this trend is not apparent until after 3.5 seconds.

From 0-1.5 seconds the ISE is nearly zero. This indicates that the simulation accurately models experimental buoy motion. The simulation does not model the effect of reflected waves on the buoy; before 1.5 seconds the reflected waves appear to have not reached the buoy, explaining why the simulation and experimental data match so well, resulting in zero ISE.

After 1.5 seconds the ISE begins to rise from zero. The slope of ISE is at its highest in the time window 1.5-3.5 seconds, indicating the initial effect of reflected waves aggressively causes the buoy to move in ways not observed in the simulation. Between 1.5 and 3.5 seconds all three plots are overlapped and the wall damping treatments do not appear to affect ISE. In fact, the data shows that more foam causes a slight increase in ISE during this time window. This could be an indication that between 1.5 and 3.5 seconds the damping treatment temporarily increases the wave field. The damping treatment could be scattering the waves more than flat tank walls do, initially creating a bustling, evanescent wave field that quickly fades.

The inverse relationship between ISE and damping thickness is confirmed after 3.5 seconds. This indicates that the buoy becomes sensitive to changes in wall damping treatment after 3.5 seconds. Although the average ISE is lower with one layer of foam than with no wall damping after 3.5 seconds, the buoy's sensitivity to changes in reflection varied with time. After 10.5 seconds, damping 1 and no wall damping plots ride very close to each other, seen in figure 13 and especially figure 14 of section 4.3. The damping effect from one layer of foam can just barely be identified after 10.5 seconds by tracking the motion of the buoy.

The decrease in ISE caused by an increase in wall damping does not appear to be a linear relationship. This is best observed by looking at the varying vertical distance between the three plots of normalized ISE in figure 14. There is one section, between 8.5-9.5 seconds, where the uniform spacing between plots indicated a linear relationship between wall damping thickness and ISE.

Overall the relationship was not linear. Between 4 and 13 seconds, the average drop in normalized ISE between no wall damping and one layer was 0.16 mm. The average drop between one layer and two was 0.62mm. That is nearly 4 times more reduction by doubling the foam thickness, i.e. adding 1.27 cm more for a total thickness of 2.54 cm.

6 Conclusion

The FDM 3D printing method is shown to be a viable alternative for the creation of model scale WECs and buoys. This work has identified an economic and readily available solution for waterproofing FDM 3D printed parts. Publishing this workflow provides a roadmap for others to consult.

It has been shown that FDM 3D printed buoys posing as surrogate model scale WECs can be used to tune wave tank damping treatments based on model specific reflections prior to deployment of fully functioning model scale WECs. In this work a sensor was made through the use of a FDM 3D printed buoy. Based on the inverse relationship observed between wall damping thickness and tank reflections sensed by the buoy, 3D printed buoys can be used, in conjunction with a tuned, non-reflective simulation, as both a sensor and an actuator to characterize model specific wave tank damping treatments. The sensitivity was not linear and required interpretation, but the buoy has been shown to successfully quantify model specific reflections in a wave tank. In this experiment, the sensitivity of the buoy acting as a sensor was close to one layer of 1.37 cm thick damping foam.

This method is recommended for quantifying reflections and tuning damping treatments to minimize reflected waves created by the initial condition response of model scale WECs. This method is further recommended for testing the forced response of model scale WECs in tanks with highly reflective surfaces. An example of a tank with highly reflective surfaces would be a common rectangular tank with wave makers on one end, beach on the other, and flat side walls. In this type of tank the presence of a model scale WEC subjected to oncoming waves from the wave makers would cast reflected waves at un-damped tank walls, creating reflection across the tank and uncertainty in the test results. Using a 3D printed surrogate buoy as a sensor provides a method for quantifying and reducing model specific reflections to meet reflection requirements before the model WEC is deployed. This issue does not apply to tanks that are fully lined with wave making/wave absorbing paddles.

6.1 Future Work

In the future, this method can be used on a larger scale to quantify reflections in the wave tank at Michigan Tech. In the Michigan Tech wave tank the effectiveness of this method can be tested under forced buoy response rather than initial condition response.

Additionally, a method for starting wave and motion data simultaneously could be developed. At this time there is an unknown delay between the start of wave data and the start of the motion data. Only from the motion data can t_1 (the time of buoy release) be identified. If the wave data and the motion data began recording simultaneously, the exact time between t_1 and t_{wg1} could be identified. This would better inform the

approximation of t_b (the time reflected waves begin to affect the buoy's motion) because t_b doesn't occur until after t_{wg1}. The results could improve the simulation by providing an updated optimization time, which is equal to t_b.

7 Reference List

[1] M. Penalba, T. Kelly, and J. V. Ringwood, "Using NEMOH for Modelling Wave Energy Converters: A Comparative Study with WAMIT," *Centre for Ocean Energy Research*.

[2] T. Havelock, "Waves due to a floating sphere making periodic heaving oscillations," pp. 1–7, Feb. 1955.

[3] "Technical Description," *wamit.com*, 2019.

[4] A. Campbell, A. Lee, A. Bentz, D. Lau, and T. Wong, "Developing an Ocean Wave Buoy to Generate Renewable Energy," Manoa Horizons, vol. 3, no. 1, pp. 21–28, Nov. 2018.

[5] L. Johanning, G. H. Smith, and J. Wolfram, "Measurements of static and dynamic mooring line damping and their importance for floating WEC devices," *Ocean Engineering*, pp. 1918–1934, Apr. 2007.

[6] D. C. Hicks and C. M. Pleass, "Wave-Powered Desalination of Seawater," 20-Dec-1983.

[7] P. Heras, S. Thomas, and M. Kramer, "Validation of Hydrodynamic Numerical Model of a Pitching Wave Energy Converter," pp. 1185–1-1185–8, Sep. 2017.

[8] M. Wu, V. Stratigaki, T. Verbrugghe, P. Troch, C. Altomare, A. Crespo, D. Kisacik, L. Cappietti, J. Dominguez, M. Hall, M. Gomez-Gesteira, P. Stansby, R. B. Canelas, and R. Ferreira, "Experimental Study of Motion and Mooring Behavior of a Floating Oscillating Water Column Wave Energy Converter," Coastlab18, pp. 1–8, May 2018.

[9] G. Payne, "Guidance for the experimental tank testing of wave energy converters," *Supergen Marine*, pp. 1–47, Dec. 2008.

[10] S. J. Beatty, B. Bocking, K. Bubbar, B. J. Buckham, and P. Wild, "Experimental and numerical comparisons of self-reacting point absorber wave energy converters in irregular waves ," *Ocean Engineering*, vol. 173, pp. 716–731, Jan. 2019.

[11] D. Elwood, S. C. Yim, J. Prudell, C. Stillinger, A. von Jouanna, T. Brekken, A. Brown, and R. Paasch, "Design, construction, and ocean testing of a taut-moored dual-body wave energy converter with a linear generator power take-off," *Renewable Energy*, vol. 35, pp. 348–354, Jul. 2009.

[12] J. R. Chaplin, F. J. M. Farley, M. E. Prentice, R. C. T. Rainey, S. J. Rimmer, and A. T. Roach, “Development of the ANACONDA all-rubber WEC,” 2007.

[13] L. Rodriguez, B. Pereiras, J. Fernandez-Oro, and F. Castro, “Optimization and experimental tests of a centrifugal turbine for an OWC device equipped with a twin turbines configuration,” *Energy*, pp. 710–720, Jan. 2019.

[14] F. Roncallo, T. Reboli, V. A. Santamaria, E. Canepa, and A. Traverso, “The Seaspoon Wave Energy Converter: performance characterization of different blade geometries,” 2017.

[15] B. Jiang, X. Li, S. Chen, Q. Xiong, B. Chen, R. Parker, and L. Zuo, “Dynamics of a hybrid ocean wave-current energy converter with mechanical motion rectifier,” Active and Passive Smart Structures and Integrated Systems XII, Mar. 2019.

[16] M. Kamarlouei, J. F. Gaspar, M. Calvário, T. S. Hallak, C. Guedes Soares, M. J. G. C. Mendes, and F. Thiebaut, “Prototyping and wave tank testing of a floating platform with point absorbers,” *Advances in Renewable Energies Offshore: Proceedings of the 3rd International Conference on Renewable Energies Offshore (RENEW 2018)*, p. 422, Oct. 2018.

[17] B. J. Rosenberg and T. R. Mundon, “Characterizing Multi-Modal 'Heave' Plates,” May 2017.

[18] D. Patterson, D. Bull, G. Bacelli, and R. Coe, “Instrumentation of a WEC Device for Controls Testing,” *Marine Energy Technology Symposium*, pp. 1–5, Apr. 2015.

[19] J. Bogaert, “Hydraulic model tests on hydrodynamic behaviour of a point absorber type wave energy converter,” *University Gent*, pp. 1–95, May 2015.

[20] B. Ding, L. S. P. da Silva, N. Sergiienko, F. Meng, J. D. Piper, L. Bennetts, M. Wagner, B. Cazzolato, and M. Arjomandi, “Study of fully submerged point absorber wave energy converter - modelling, simulation and scaled experiment,” Apr. 2017.

[21] J. C. McNatt, “Cylindrical Linear Water Waves and their Application to the Wave-body Problem,” thesis, 2015.

[22] M. W. Kim, W. Koo, and S. Y. Hong, “Numerical analysis of various artificial damping schemes in a three-dimensional numerical wave tank,” Ocean Engineering, pp. 165–173, Nov. 2013.

[23] J. R. M. Taylor, M. Rea, and D. J. Rogers, “The Edinburgh curved tank,” *5th European Wave Energy Conference, Cork, Ireland*, pp. 307–314, Sep. 2003.

[24] H. A. Schaffer and G. Klopman, “Review of Multidirectional Active Wave Absorption Methods,” pp. 88–97, Apr. 2000.

[25] Y. Cao, R. F. Beck, and W. W. Schultz, “An Absorbing Beach for Numerical Simulations of Nonlinear Waves in a Wave Tank,” pp. 17–20.

[26] I. H. Cho and M. H. Kim, “Wave absorbing system using inclined perforated plates,” vol. 608, pp. 1–20, 2008.

[27] U. A. Korde and J. V. Ringwood, *Hydrodynamic control of wave energy devices*. Cambridge: Cambridge University Press, 2016.

[28] F. Calignano, D. Manfredi, E. P. Ambrosio, S. Biamino, M. Lombardi, E. Atzeni, A. Salmi, P. Minetola, L. Iuliano, and P. Fino, “Overview on Additive Manufacturing Technologies,” vol. 105, no. 4, pp. 593–612, Apr. 2017.

A Appendix

A.1 Experimental Standard Operating Procedure

The following steps were taken to complete one experimental run as shown in section 3.4.

1. Buoy positioned at the center of the polycarbonate inner ring with in the tank
2. Mooring line fixed to hold the buoy at a submersion level of 1 cm below its natural draft
3. Quick release mechanism engaged
4. Buoy left to settle at least 2 minute to allow water surface and buoy to become still so that the initial conditions had no waves and no buoy movement.
5. Wave gauge and motion tracking software capture initiated
6. Quick release mechanism triggered
7. Wave gauge and motion tracking software capture stopped after 15 seconds

A.2 Simulation

Figure A.2.1 below shows the layout of the simulation used in conjunction with the 3D printed buoy to quantify wave tank reflections. A description of this simulation can be found in section 2.

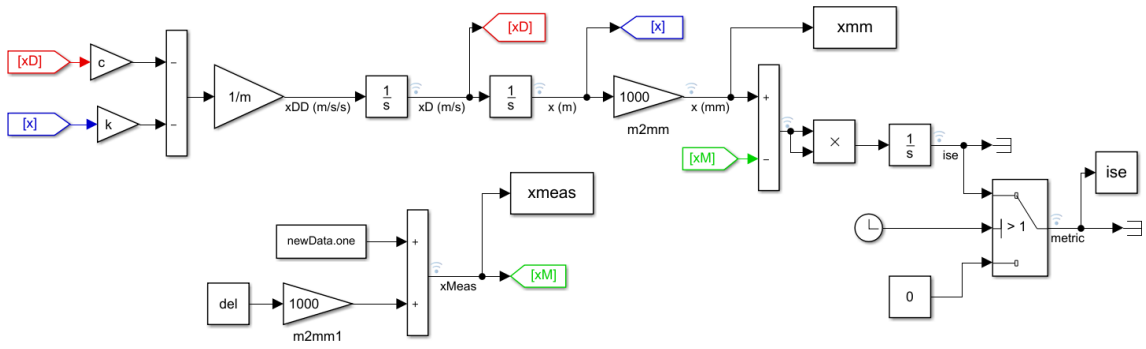

Figure A.2. 1. Simulink block diagram

A.3 Buoy Geometry

The dimensioned drawings below represent the two part 3D printed buoy used in this work. Figure A.3.1 is a CAD drawing of the buoy's lid and figure A.3.2. is the buoy itself. Both parts were printed from ABS plastic.

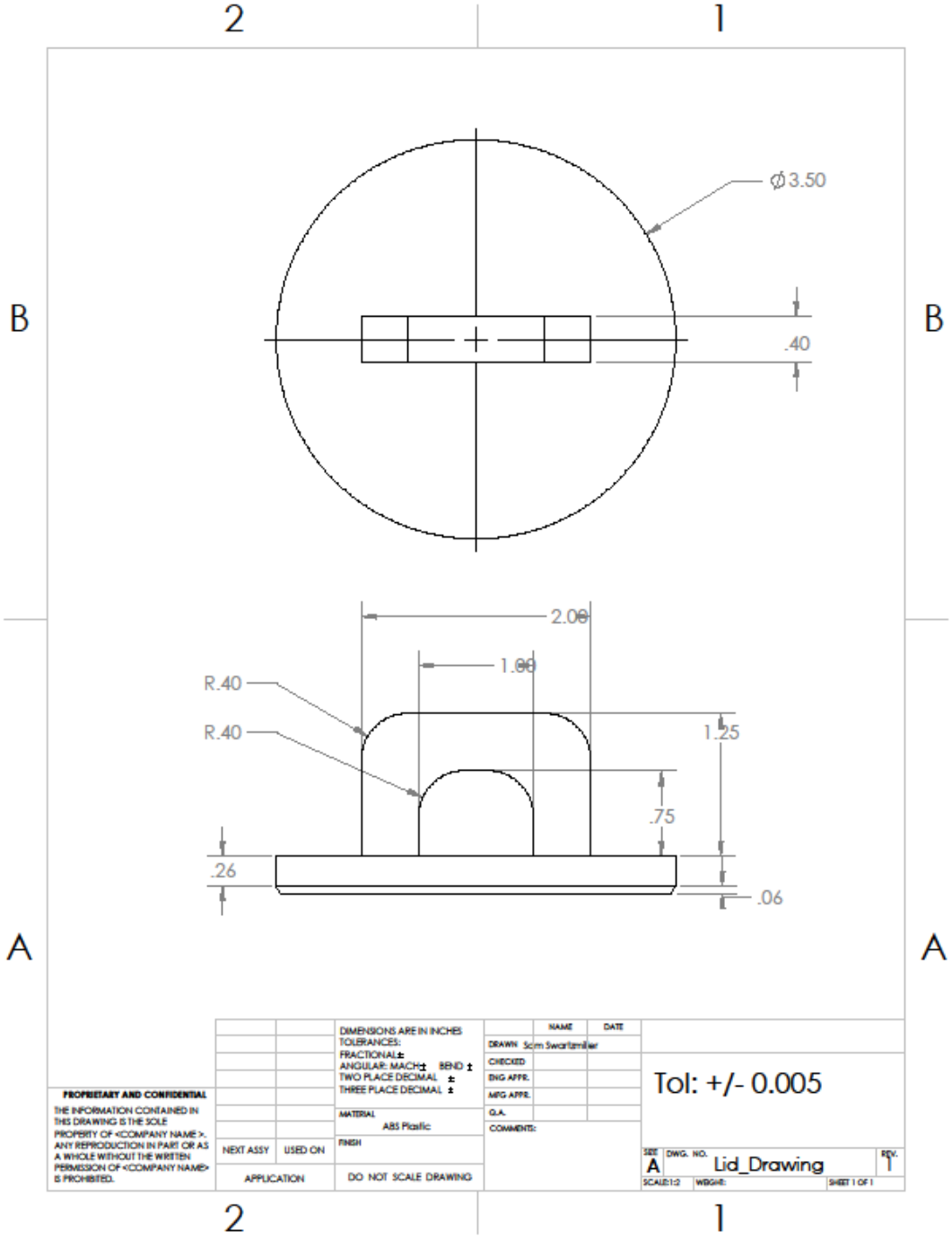

Figure A.3. 1. CAD drawing of buoy lid

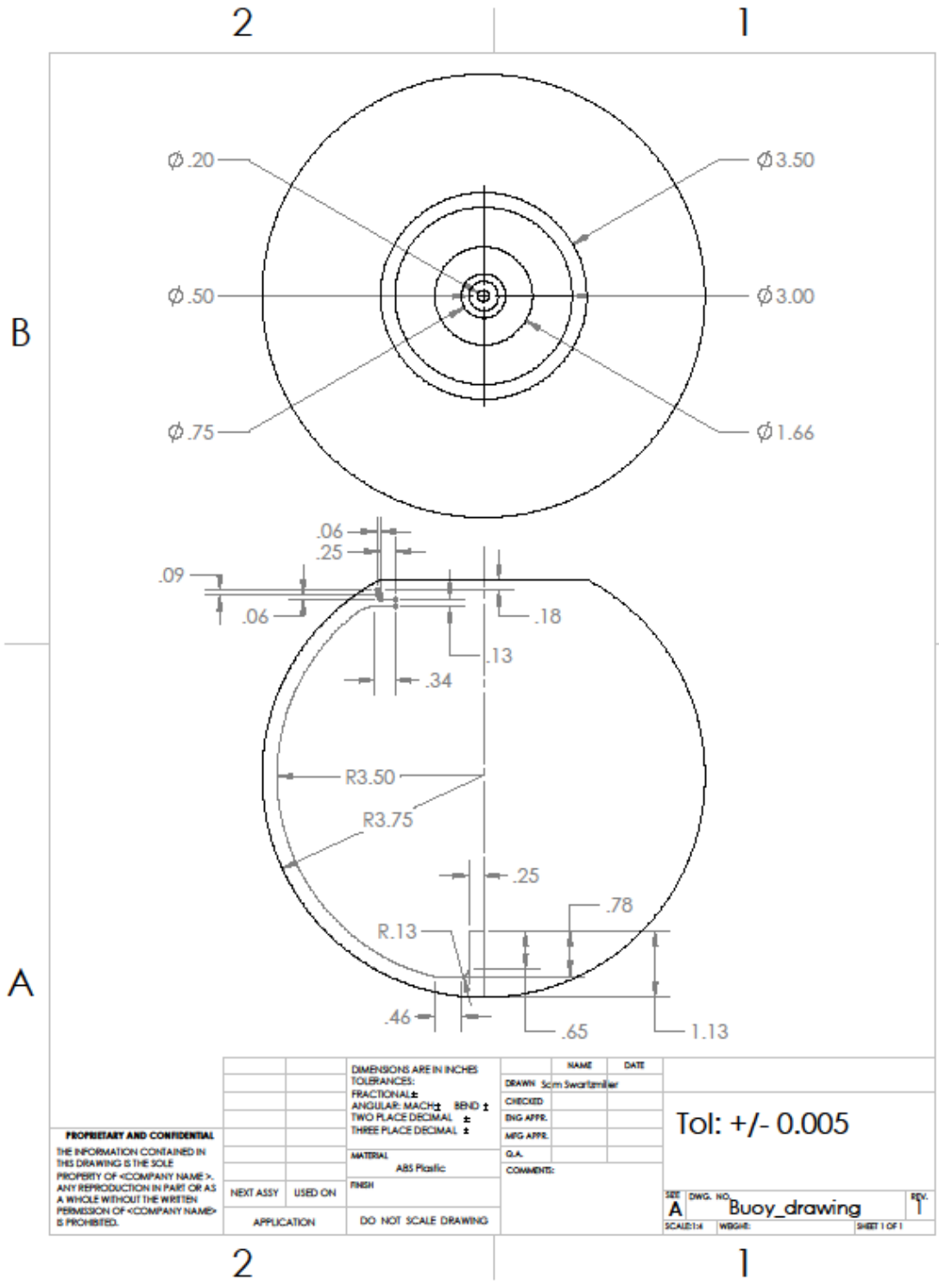

Figure A.3. 2. CAD drawing of buoy body

B Copyright documentation

There is no copyrighted material in this document.